International Journal of Science and Research (IJSR)
ISSN: 2319-7064
Impact Factor 2024: 7.101

DFT Calculation and *in silico* ADMET Studies of Syringaldehyde 4-hydroxy-3,5-Dimethoxybenzaldehyde (6-chloropyridazin-3-yl) Hydrazone Hydrate

U. Muhammed Rafi

Post-Graduate and Research Department of Chemistry, The New College, University of Madras, Chennai 600 014, India
Corresponding Author Email: *muhammedraffi[at]gmail.com*

Abstract: ***This study presents an analysis of 3-Chloro-6-(4-hydroxy-3,5-dimethoxybenzylidenehydrazinyl)pyridazine, employing a multifaceted approach that integrates NMR spectroscopy, Density Functional Theory (DFT) and in silico pharmacokinetic analysis, to explore their nuclear resonance, electronic and pharmacokinetic properties. Utilizing DFT analysis with the B3LYP functional and the 6-311++G(d,p) basis set, molecular geometries were optimized, offering insights into the molecular structure and stability of the compound. Frontier Molecular Orbital (FMO) analysis revealed the stability level of the compound. The band gap energy and chemical reactivity parameters were also computed. Chemical potential and hardness analyses highlighted stronger binding affinity for the compound, suggesting stronger potential interactions. In silico ADME study was also performed and the results suggested the presence of high drug-likeness of the synthesized compound. This study underscores the promising role of this compound in providing a solid foundation for future drug development and optimization efforts.***

Keywords: Pyridazine; Syringaldehyde; HOMO-LUMO; Pharmacokinetics

1. Introduction

Pyridazine has wide applications in drug design [1], agrochemical activities [2] and has also been used as ligands in coordination chemistry. There have been numerous systems such as acyclic ligands [3], coordination polymers [4], cryptands [5] and also macrocycles [6] in which pyridazine units have been incorporated. Pyridazine derivatives have been the subject of extensive study in recent years, and the results have demonstrated a broad spectrum of pharmacological actions, including antidepressant [7], COX-2 inhibitor [8] and anticancer properties [9, 10]. The introduction of new substituents or functional groups at various positions on aromatic or heteroaromatic fragments of a potential drug may cause changes in its molecular shape, allowing for optimal receptor binding, as well as changes in its physicochemical properties, which affect drug distribution and metabolism [11]. When compared to pyridine systems, the distinct electronic ligand characteristics can be expected to result in a distinct chemical behavior. Pyridazine's two N-donor atoms reduce its electron donor capabilities in comparison to pyridine; this is demonstrated by the significantly lower pKa values (2.24 for parent pyridazine and 5.25 for pyridine) [12]. With the recent discovery of compounds that may be used as medicines, pyridazines and their derivatives have drawn a lot of attention due to their structural significance in a number of physiologically active compounds [13, 14]. Antimicrobial activity against Gram (+ve) (Staphylococcus aureus and Streptococcus faecalis) and Gram (-ve) (Escherichia coli and Pseudomonas aeruginosa) bacteria was shown by 1-[4-(2-methoxybenzyl)-6-arylpyridazin-3(2H)-ylidene]hydrazines during screening [15]. In comparison to the common medications nevirapine and delavirdine, diarylpyridazine derivatives with substituents of 2,6-dibromo-4-methyl and p-CN were found to be highly effective in inhibiting HIV-1 (Human Immunodeficiency Virus type 1) IIIB in MT-4 cells [16].

The current research has focused on a heterocyclic compound containing a pyridazine unit, which is a part of our research on the synthesis of pyridazine compounds, exhibiting biological and pharmacological activities. Single crystal X-ray diffraction analysis has already determined the crystal structure of the compound and reported in the literature [17]. Theoretical calculations based on the DFT approach were used to compare the structural parameters and to obtain additional information on the reactivity descriptors of the compound. Recently, *in silico* ADMET profiles are often used to ascertain whether a compound can get to its target site, hence pharmacological profile of the compound was evaluated through an analysis of drug-likeness, bioactivity and Lipinski's violation of 5.

2. Experimental Section

2.1 Materials and instrumentation

The compound (**1**) was synthesized by following the procedure as described in the literature [17]. Bruker Avance spectrometer was used to record NMR spectra of the compound using DMSO-d_6 as solvent (400 MHz for ^{1}H and 100 MHz for ^{13}C NMR) at room temperature and chemical shift values were expressed in δ values (ppm) relative to tetramethyl silane (TMS) as an internal standard.

^{1}H NMR (400 MHz, DMSO-d_6): δ 11.579 (s, 1H, NH), 8.765 (s, 1H, azomethine –CH=N), 8.005 (s, 1H, phenolic proton), 7.614 –7.684 (*d*, 2H, Ar_{pdz}–H), 6.966 (*s*, 1H, Ar–H), 3.819 (*s*, 6H, OCH_3). ^{13}C NMR (100 MHz, DMSO-d_6): δ 159.41, 148.64, 143.16, 137.67, 130.34, 125.48, 116.24, 104.48, 56.49.

2.2 Computational details

The molecular orbital calculations of the compound were carried out by employing the density functional theory (DFT) at B3LYP level and 6-31G (d,p) basis set [18] using the Gaussian 03 software package in the gas phase [19].

2.3 Prediction of pharmacokinetic parameters

Pharmacokinetic properties (Absorption, Distribution, Metabolism and Excretion) of the compound was calculated through SwissADME (http://www.swissadme.ch/index.php), Molinspiration (https://molinspiration.com/cgi/properties) and admet SAR prediction tool (http://lmmd.ecust.edu.cn/admetsar1/predict/) web portals [20-22].

3. Results and discussion

3.1 NMR spectroscopy

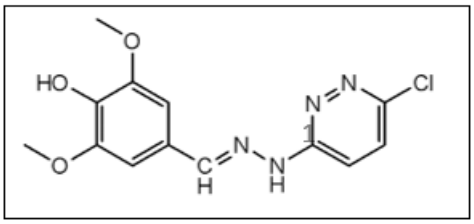

The ^{1}H and ^{13}C NMR spectrum are shown in (**Fig. 1 & 2**). The appearance of a signal around 8.765 ppm is due to formation of the imine moiety and a peak at 4.40 ppm not observed suggest the disappearance of the primary amine group. The aromatic protons of the pyridazine and phenolic rings were observed as a quartet in the region 7.614–7.684 ppm and as a singlet at 6.966 ppm, respectively. The presence of two methoxy substituents and a phenolic hydroxyl group is evidenced by a singlet peak at 3.819 ppm and at 8.005 ppm, respectively. The ^{13}C NMR spectrum of the compound was characterized by the presence of a characteristic signal at 159.41 ppm for the azomethine carbon (C=N) and absence of a signal at 198 ppm corresponding to an aldehyde group. The spectrum was further characterized by the peaks in the range of 148.64−104.48 ppm due to carbons of phenyl ring and by the peaks at 56.49 ppm corresponding to methoxy carbons.

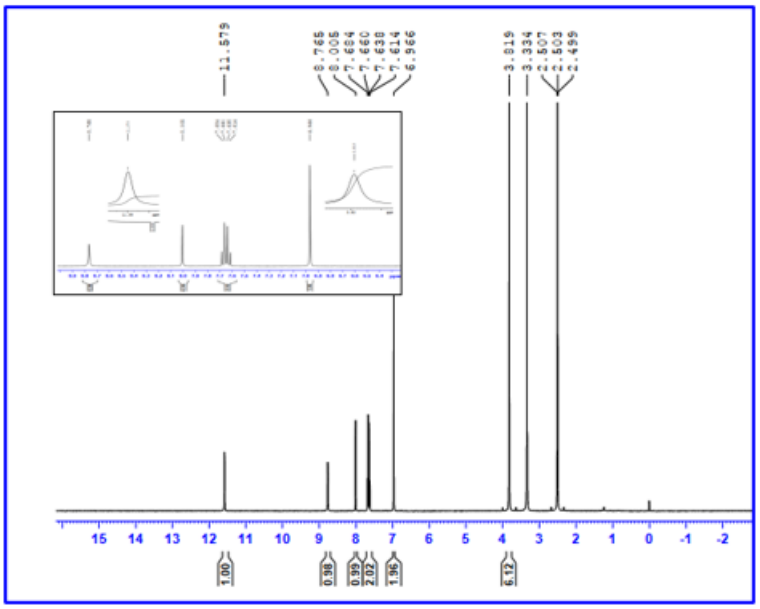

Figure 1: ^{1}H NMR spectrum of the compound (**1**).

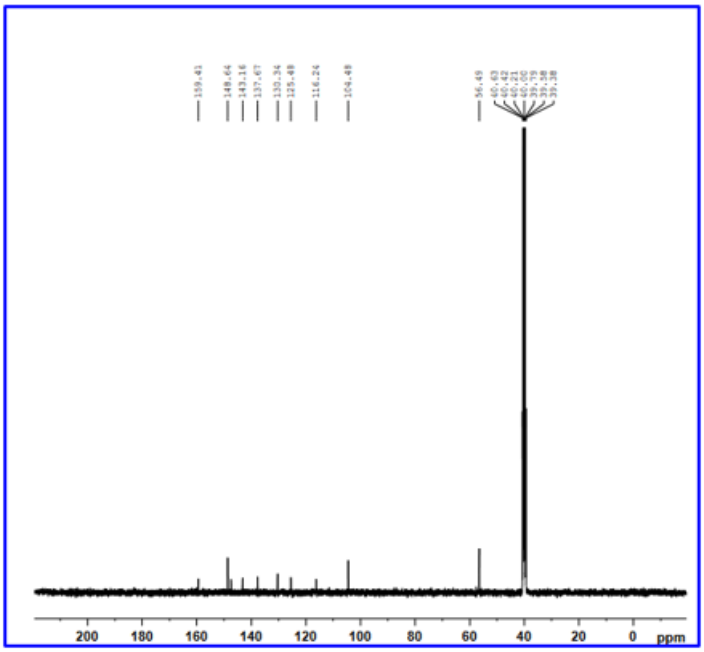

Figure 2: ^{13}C NMR spectrum of the compound (**1**).

3.2. Molecular geometry

The compound (**1**) was optimized through the B3LYP / 6-31+G(d,p) level of calculation in the gas phase. As the crystallographic data of the compound (**1**) was available [17], the important bond length and bond angle parameters of the compound obtained from DFT calculations were compared with the crystallographic data. The compound under investigation corresponds to *C1* point group symmetry. The computational and experimental values of the selected structural parameters including bond lengths and bond angles are listed in **Table 1**, and the optimized geometry structure of the compound is shown in **Fig. 3**. The identified bond lengths were good reliable with the experimental parameters and the deviations could take place due to the intramolecular hydrogen bonding interactions. In general, the calculated bond lengths are typically longer than the experimental data because the former are optimized in the gas phase while the latter are in a tight crystal lattice. It was concluded that the sequences of B3LYP functional with both 6-31+ G(d,p) basis sets have produced compatible results with the experimental values. The compound has been computed to have a dipole moment of 6.79 B.M.

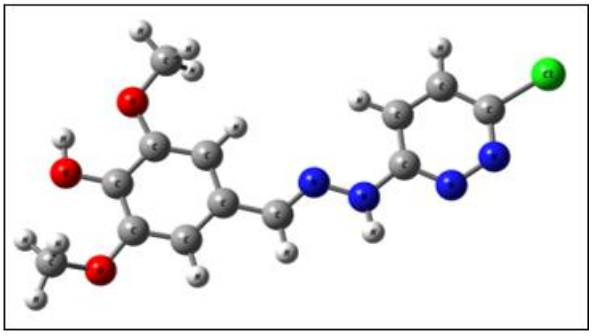

Figure 3: The optimized geometry structure of the compound (**1**) utilizing B3LYP / 6-31+G(d,p) level of calculation.

Table 1: B3LYP/GEN and B3LYP/LANL2DZ Bond lengths (Å), Bond angles (°) and Torsion angles (°) of the compound (**1**)

Parameters	Experimental values [17]	Theoretical values	Parameters	Experimental values [17]	Theoretical values
Bond length (Å)			**Bond angle (°)**		
C(1)-N(1)	1.301(3)	1.325	N(1)-C(1)-C(2)	124.45(18)	124.35
C(1)-C(2)	1.394(3)	1.405	N(1)-C(1)-Cl(1)	115.48(14)	116.53
C(1)-Cl(1)	1.7391(19)	1.816	C(2)-C(1)-Cl(1)	120.06(16)	119.11
C(2)-C(3)	1.364(3)	1.381	C(3)-C(2)-C(1)	117.15(19)	117.17
C(2)-H(2)	0.9300	1.082	C(3)-C(2)-H(2)	121.4	122.02
C(3)-C(4)	1.401(3)	1.414	C(1)-C(2)-H(2)	121.4	120.80
C(3)-H(3)	0.9300	1.081	C(2)-C(3)-C(4)	117.61(17)	116.98
C(4)-N(2)	1.341(2)	1.357	C(2)-C(3)-H(3)	121.2	122.90
C(4)-N(3)	1.354(2)	1.374	C(4)-C(3)-H(3)	121.2	120.11
C(5)-N(4)	1.278(2)	1.299	N(2)-C(4)-N(3)	113.43(16)	113.94
C(5)-C(6)	1.461(2)	1.457	N(2)-C(4)-C(3)	121.84(17)	123.10
C(5)-H(5)	0.9300	1.095	N(3)-C(4)-C(3)	124.73(15)	122.59
C(6)-C(11)	1.392(2)	1.414	N(4)-C(5)-C(6)	122.67(16)	122.43
C(6)-C(7)	1.396(2)	1.403	N(4)-C(5)-H(5)	118.7	120.96
C(7)-C(8)	1.385(2)	1.400	C(6)-C(5)-H(5)	118.7	116.61
C(7)-H(7)	0.9300	1.084	C(11)-C(6)-C(7)	120.11(14)	119.53
C(8)-O(1)	1.371(2)	1.388	C(11)-C(6)-C(5)	122.13(15)	121.55

C(8)-C(9)	1.387(2)	1.399	C(7)-C(6)-C(5)	117.76(15)	118.92
C(9)-O(2)	1.3660(18)	1.385	C(8)-C(7)-C(6)	119.90(15)	121.41
C(9)-C(10)	1.399(2)	1.411	C(6)-C(7)-H(7)	120.0	121.13
C(10)-O(3)	1.3639(18)	1.398	C(7)-C(8)-C(9)	120.37(15)	119.04
C(10)-C(11)	1.385(2)	1.385	C(8)-C(9)-C(10)	119.54(13)	119.34
N(1)-N(2)	1.350(2)	1.356	O(3)-C(10)-C(11)	125.42(14)	125.9
N(3)-N(4)	1.3776(18)	1.370	O(3)-C(10)-C(9)	114.13(13)	112.23
Torsion angle (°)			C(11)-C(10)-C(9)	120.45(14)	121.86
N(1)-C(1)-C(2)-C(3)	1.1(3)	0.01	C(10)-C(11)-C(6)	119.62(14)	118.78
Cl(1)-C(1)-C(2)-C(3)	-177.79(14)	-179.98	C(10)-C(11)-H(11)	120.2	122.06
C(1)-C(2)-C(3)-C(4)	-0.7(3)	0.003	C(6)-C(11)-H(11)	120.2	119.16
C(2)-C(3)-C(4)-N(2)	-0.6(3)	-0.016	H(12A)-C(12)-H(12B)	109.5	110.04
N(4)-C(5)-C(6)-C(11)	1.3(3)	0.599	O(3)-C(12)-H(12C)	109.5	110.77
N(4)-C(5)-C(6)-C(7)	-179.92(16)	-178.87	H(12A)-C(12)-H(12C)	109.5	109.96
C(11)-C(6)-C(7)-C(8)	-0.3(2)	0.546	H(12B)-C(12)-H(12C)	109.5	109.83
C(5)-C(6)-C(7)-C(8)	-179.14(15)	-179.97	O(1)-C(13)-H(13A)	109.5	110.36
C(6)-C(7)-C(8)-C(9)	0.4(3)	0.368	H(13A)-C(13)-H(13B)	109.5	109.92
O(1)-C(8)-C(9)-O(2)	-0.9(2)	1.65	O(1)-C(13)-H(13C)	109.5	111.12
C(7)-C(8)-C(9)-O(2)	178.79(15)	178.06	H(13A)-C(13)-H(13C)	109.5	109.84
O(1)-C(8)-C(9)-C(10)	-179.39(15)	-177.61	H(13B)-C(13)-H(13C)	109.5	111.02
O(2)-C(9)-C(10)-O(3)	0.5(2)	1.209	C(1)-N(1)-N(2)	118.87(15)	119.40
O(2)-C(9)-C(10)-C(11)	-179.64(15)	-178.11	C(4)-N(2)-N(1)	120.06(16)	118.99
C(8)-C(9)-C(10)-C(11)	-1.2(2)	1.16	C(4)-N(3)-N(4)	121.33(16)	121.40
O(3)-C(10)-C(11)-C(6)	-178.81(15)	-179.27	C(8)-O(1)-C(13)	118.43(15)	119.64
C(9)-C(10)-C(11)-C(6)	1.4(2)	-0.246	C(9)-O(2)-H(2O)	109.9(16)	108.32
C(7)-C(6)-C(11)-C(10)	-0.6(2)	-0.603	C(10)-O(3)-C(12)	117.62(13)	118.81

3.3 Frontier molecular orbitals (FMOs) analysis

The highest occupied molecular orbital (HOMO) and lowest unoccupied molecular orbital (LUMO) make up the Frontier Molecular Orbitals (FMOs). FMOs have an important role in the study of electrical and optical properties of a compound. The HOMO-LUMO gap quantifies the chemical stability of molecules and a larger gap implies that a molecule is more stable and therefore less reactive [23]. The DFT calculation was done using B3LYP functional, supplemented with the standard 6-31G (d,p) basis set in gas phase, which computed the E_{HOMO} value has –7.57 eV, while E_{LUMO} value has –5.02 eV, and the band gap, ΔE value has 2.55 eV for the compound (**Fig. 4**). The compound exhibited a small HOMO−LUMO energy gap, indicating its semiconductor nature, as the observed band gap matches with the well-established band gap energy of semiconductors (<3 eV) [24].

Using Koopman's theorem, the E_{HOMO} and E_{LUMO} values can be applied to determine the global chemical reactivity descriptors such as chemical potential (μ), hardness (η), softness (S) and electrophilicity index (ω) , which were deduced from ionization potential (IP = $-E_{HOMO}$) and electron affinity (EA = $-E_{LUMO}$) values and the calculated chemical reactivity descriptor values were summarized in **Table 2**. Further, the compound has high chemical potential and electrophilicity index value, which indicates that the compound to be chemically and biologically active.

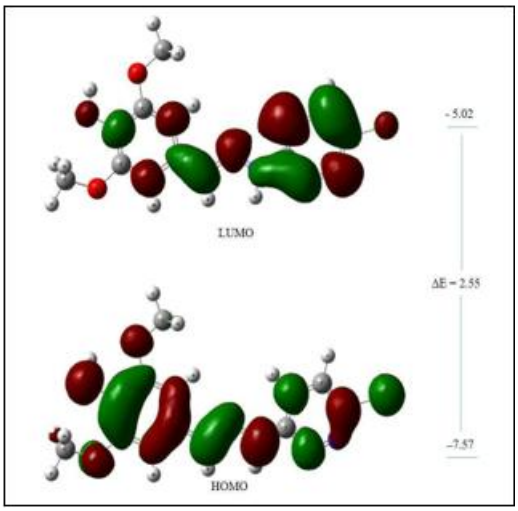

Figure 4: Frontier molecular (HOMO and LUMO) plots of the compound (**1**) obtained by the B3LYP / 6-31+G(d,p) method.

Table 2: Calculated HOMO−LUMO Energy Gap, Chemical potential (μ), chemical hardness (η), softness (S) and electrophilicity (ω) values of the compound (**1**) calculated by the DFT method.

Parameters	Values (eV)	Parameters	Values (eV)
Energy band gap	2.55	Chemical Hardness	1.27
Ionization potential	7.57	Chemical potential	–6.29
Electron affinity	5.02	Softness	0.39
Electronegativity	6.29	Electrophilicity index	15.54

3.4 In silico pharmacokinetics studies

The key parameters in drug discovery are pharmacokinetics and toxicological studies. The compound (1) complied with Lipinski's rule of five [25] for the prediction of drug-likeness of the compound. The drug molecules of higher molecular weight are not readily transported and have poor absorption

compared to molecules with low molecular weight [26]. The compound has a molecular weight of 308.7, which is less than 500 Da and the TPSA value is also low, indicating the compound can easily cross cell membranes. The high lipophilicity expressed as LogP is 1.98, which indicates that the compound has good absorption or permeation across the cell membrane. The absorption percentage (AB%) was calculated using the following formula [27];

$$AB\% = 109 - (0.345 \times TPSA)$$

The compound possessed AB% greater than 50%, which indicates the compound to have proper bioavailability, distribution and circulation by oral route [21, 28]. A positive drug-likeness score was assessed for the compound (**Table 3**), which indicates that the compound can act as a potential drug candidate.

Table 3: Drug-likeness profiles of compound (**1**) were evaluated by Lipinski's 'rule of five' using the SwissADME web-server tool.

Compound	Mass (< 500)	Hydrogen bond donor (< 5)	Hydrogen bond Acceptor (< 10)	LogP (< 5)	TPSA (≤ 140)	Absorption percentage (AB%) (> 50%)	Drug likeness Score (> 0)
1	308.7	2	6	1.98	88.86	78.34	0.55

Molinspiration was employed to determine the activity of the compound (**1**) against G-protein coupled receptor ligand (GPCRL), ion channel modulator (ICM), kinase inhibitor (KI), nuclear receptor ligand (NRL), protease inhibitor (PI), and enzyme inhibitor (EI) in addition to verifying the bioactivity scores of the compound [22]. A bioactivity score > 0 indicates significant biological activity, while a score between −0.50 and 0.00 indicates moderate biological activity, and a score < −5.0 indicates inactivity for the compound under consideration [29]. The compound demonstrated moderate biological potential against GPCRL, ICM, KI and EI (**Table 4**). Based on the observed values, the compound was evaluated as a better kinase and enzyme inhibitor and can be used to develop drugs for diseases caused by kinase dysregulation, such as cancer, diabetes and inflammation.

Table 4: Bioactivity scores prediction of the compound (**1**) by Molinspiration

Compound	GPCRL	ICM	KI	NRL	PI	EI
1	−0.44	−0.44	−0.33	−0.98	−0.82	−0.25

To understand the physicochemical interactions and drug-likeness properties of the compound, the ADMET properties of the compound (**1**) were predicted using the admetSAR prediction tool. **Table 5** lists the main objectives of the ADMET study, which indicates that the compound showed optimal solubility (LogS) with values higher than −4 (> −4) [21]. The compound has an excellent human intestinal absorption (HIA) value of 0.88, indicating that it may be better absorbed from the intestinal tract after oral administration. The compound also had a better Blood Brain Barrier (BBB) value of 0.80 and Caco-2 permeability value of 0.55. The optimal LD50 value indicates that the compound is not lethal. Finally, the ADMET properties showed that the compound to be non-AMES toxic and non-carcinogenic in nature.

Table 5: ADMET prediction profile of the compound (**1**) through admetSAR.

Compound	Log S (> −4)	Blood Brain Barrier (BBB)	Human intestinal absorption (HIA)	Caco-2 permeability	Ames toxicity	Carcinogenicity	LD_{50} (rat acute toxicity) (mol/kg)
1	−3.85	0.8	0.88	0.55	Non-toxic	Non-carcinogen	2.42

4. Conclusion

Using the DFT method, the HOMO-LUMO calculations were carried out, which indicated the compound (**1**) to have better biological activity and the band gap value was within the acceptable range of organic semiconductors, which indicated the semiconductor nature of the compound. Pharmacokinetics profiling using Lipinski's 'rule of five' and ADMET studies predicted the drug-likeness and nontoxicity of the compound. The pharmacokinetic evaluation suggested that the compound might function as a more potent kinase inhibitor, making it a promising treatment option for cancer. Future research will focus on synthesis of metal complexes using the synthesized compound as the ligand and will look into the potential of the compound and its metal complexes for *in vitro* biological studies.

Conflicts of interest

The authors declare that they have no known conflict of interest.

Acknowledgements

The authors thank Vellore Institute of Technology (VIT) for recording NMR spectral data.

References

[1] Roth GJ, A. Heckel, Kley JT, Lehmann T, Müller SG, Oost T, Rudolf K, Arndt K, Budzinski R, Lenter M, Lotz RRH, Schindler M, Thomas L, Stenkamp D. Design, synthesis and evaluation of MCH receptor 1 antagonists—Part II: Optimization of pyridazines toward reduced phospholipidosis and hERG inhibition. Bioorg. Med. Chem. Lett. 2015 Aug; 25 (16): 3270-3274. https://doi.org/10.1016/j.bmcl.2015.05.074

[2] Jones FW. Fiber-reactive insecticides for wool: organophosphorus esters of nitrogen heterocycles. J. Agric. Food Chem. 1983 Mar; 31 (2): 190-194. https://doi.org/10.1021/jf00116a002

[3] Guo LY, Zhang XL, Wang HS, Liu C, Li ZG, Liao ZJ, Mi BX, Zhou XH, Zheng C, Li YH, Gao ZQ. New homoleptic iridium complexes with C^N=N type ligand

for high efficiency orange and single emissive-layer white OLEDs. J. Mater. Chem. C 2015 Jun; 3 (21): 5412-5418. https://doi.org/10.1039/C5TC00458F

[4] Jess I, Nather C. Synthesis, Crystal Structures, and Thermal and Thermodynamic Properties of Dimorphic Copper(I) Coordination Polymers, Inorg. Chem. 2003 Apr; 42 (9): 2968-2976. https://doi.org/10.1021/ic026181i

[5] Brooker S, Ewing JD, Ronson TK, Harding CJ, Nelson J, Speed DJ. Redox-Adaptable Copper Hosts. Pyridazine-Linked Cryptands Accommodate Copper in a Range of Redox States. Inorg. Chem. 2003 Mar; 42 (8): 2764-2773. https://doi.org/10.1021/ic0261124

[6] Brooker S, Hay SJ, Plieger PJ. A Grid Complex $[CuL_2]^{4+}$ and a Mixed-Valent Complex $[Cu^{II}Cu^{I}L(MeCN)_2]^{3+}$ of the Pyridazine-Containing Macrocycle L. Angew. Chem. Int. Ed. 2000 Jun; 39 (11): 1968-1970. https://doi.org/10.1002/1521-3773(20000602)39:11<1968::AID-ANIE1968>3.0.CO;2-2

[7] Komkov AV, Komendantova AS, Menchikov LG, Chernoburova EI, Volkova YA, Zavarzin IV. A Straightforward Approach toward Multifunctionalized Pyridazines via Imination/Electrocyclization. Org Lett 2015 Jul; 17 (15): 3734–3737. https://doi.org/10.1021/acs.orglett.5b01718

[8] Harris RR, Black L, Surapaneni S, Kolasa T, Majest S, Namovic MT, Grayson G, Komater V, Wilcox D, King L, Marsh K, Jarvis MF, Nuss N, Nellans H, Pruesser L, Reinhart GA, Cox B, Jacobson P, Stewart A, Coghlan M, Carter G, Bell RL. ABT-963 [2-(3,4-Difluoro-phenyl)-4-(3-hydroxy-3-methyl-butoxy)-5-(4-methanesulfonyl-phenyl)-2H-pyridazin-3-one], A Highly Potent and Selective Disubstituted Pyridazinone Cyclooxgenase-2 Inhibitor. J Pharmacol Exp Ther 2004 Dec; 311(3): 904–912. https://doi.org/10.1124/jpet.104.070052

[9] Rafi UM, Mahendiran D, Kumar RS, Rahiman AK. In vitro anti-proliferative and in silico docking studies of heteroleptic copper(II) complexes of pyridazine-based ligands and ciprofloxacin. Appl Organometal Chem 2019 Apr; 33: e4946. https://doi.org/10.1002/aoc.4946

[10] Ahmad S, Rathish IG, Bano S, Alam MS, Javed KK. Synthesis and biological evaluation of some novel 6-aryl-2-(p-sulfamylphenyl)-4,5-dihydropyridazin-3(2H)-ones as anti-cancer, antimicrobial, and anti-inflammatory agents. J Enzyme Inhib Med Chem 2019 Jun; 25 (2): 266–271. https://doi.org/10.3109/14756360903155781

[11] Piatnitski EL, Duncton MA, Kiselyov AS, Katoch-Rouse R, Sherman D, Milligan DL, Balagtas C, Wong WC, Kawakami J, Doody JF. Arylphthalazines: Identification of a new phthalazine chemotype as inhibitors of VEGFR kinase. Bioorg. Med. Chem. Lett. 2005 Nov; 15 (21): 4696-4698. https://doi.org/10.1016/j.bmcl.2005.07.064

[12] Lide DR, CRC Handbook of Chemistry and Physics, Taylor & Francis, Boca Raton, 88th edn., 2007.

[13] Contreras JM, Rival YM, Chayer S, Bourguignon JJ, Wermuth CG. Aminopyridazines as Acetylcholinesterase Inhibitors. J Med Chem 1999 Feb; 42 (4)**:**730–741. https://doi.org/10.1021/jm981101z

[14] Olmo E del, Barboza B, Ybarra MI, López-Pérez JL, Carrón R, Sevilla MA, Boselli C, Feliciano AS. Vasorelaxant activity of phthalazinones and related compounds. Bioorg Med Chem Lett 2006 May; 16 (10): 2786–2790. https://doi.org/10.1016/j.bmcl.2006.02.003

[15] Kandile NG, Mohamed MI, Zaky H, Mohamed HM. Novel pyridazine derivatives: Synthesis and antimicrobial activity evaluation, Eur. J. Med. Chem. 2009 May; 44 (5): 1989-1996. https://doi.org/10.1016/j.ejmech.2008.09.047

[16] Li D, Zhan P, Liu H, Pannecouque C, Balzarini J, Clercq ED, Liu X. Synthesis and biological evaluation of pyridazine derivatives as novel HIV-1 NNRTIs. Bioorg. Med. Chem. 2013 Apr, 21 (7), 2128-2134. https://doi.org/10.1016/j.bmc.2012.12.049

[17] Ummer, M. R., NizamMohideen, M., Noorulla, M. N. & Moolan Khaja, A. S. (2025). Synthesis, crystal structure, and in silico mol-ecular docking studies of 4-hy-dr-oxy-3,5-di-meth--oxy-benzaldehyde(6-chloro-pyridazin-3-yl)hydrazine monohydrate. Acta Cryst. 2025 Mar; E81, 336-340. https://doi.org/10.1107/S205698902500252X

[18] Becke AD. Density-functional thermochemistry. III. The role of exact exchange. J. Chem. Phys. 1993 Apr; 98 (7): 5648–5652. http://dx.doi.org/10.1063/1.464913

[19] Frisch MJ, Trucks GW, Schlegel HB, Scuseria GE, Robb MA, Cheeseman JR, Montgomery Jr JA, Vreven T, Kudin KN, Burant JC, Millam JM, Iyengar SS, Tomasi J, Barone V, Mennucci B, Cossi M, Scalmani G, Rega N, Petersson GA, Nakatsuji H, Hada M, Ehara M, Toyota K, Fukuda R, Hasegawa J, Ishida M, Nakajima T, Honda Y, Kitao O, Nakai H, Klene M, Li X, Knox JE, Hratchian HP, Cross JB, Bakken V, Adamo C, Jaramillo J, Gomperts R, Stratmann RE, Yazyev O, Austin AJ, Cammi R, Pomelli C, Ochterski JW, Ayala PY, Morokuma K, Voth GA, Salvador P, Dannenberg JJ, Zakrzewski VG, Dapprich S, Daniels AD, Strain MC, Farkas O, Malick DK, Rabuck AD, Raghavachari K, Foresman JB, Ortiz JV, Cui Q, Baboul AG, Clifford S, Cioslowski J, Stefanov BB, Liu G, Liashenko A, Piskorz P, Komaromi I, Martin RL, Fox DJ, Keith T, Al-Laham MA, Peng CY, Nanayakkara A, Challacombe M, Gill PMW, Johnson B, Chen W, Wong MW, Gonzalez C, Pople JA (2004) Gaussian 03 Revision C.02 Gaussian Inc Wallingford CT.

[20] Daina A, Michielin O, Zoete V. SwissADME: a free web tool to evaluate pharmacokinetics, drug-likeness and medicinal chemistry friendliness of small molecules. Sci Rep 2017 Mar; 7: 42717. https://doi.org/10.1038/srep42717

[21] Cheng F, Li W, Zhou Y, Shen J, Wu Z, Liu G, Lee PW, Tang Y. admetSAR: A comprehensive source and free tool for assessment of chemical ADMET properties. J. Chem. Inf. Model. 2012 Oct; 52(11): 3099–3105. https://doi.org/10.1021/ci300367a

[22] Bhowmik D, Nandi R, Jagadeesan R, Kumar N, Prakash A, Kumar D. Identification of potential inhibitors against SARS-CoV-2 by targeting proteins responsible for envelope formation and virion assembly using docking based virtual screening, and pharmacokinetics approaches. Infect Genet Evol 2020 Oct; 84:104451. https://doi.org/10.1016/j.meegid.2020.104451

[23] Thanikaivelan P, Subramanian V, Rao JR, Nair BU. Application of quantum chemical descriptor in quantitative structure activity and structure property relationship. Chem Phys Lett 2000 Jun; 323 (1-2): 59–70. https://doi.org/10.1016/S0009-2614(00)00488-7
[24] Costa JC, Taveira RJ, Lima CF, Mendes A, Santos LM (2016) Optical band gaps of organic semiconductor materials. Opt Mater 58:51–60. https://doi.org/10.1016/j.optmat.2016.03.041.
[25] Lipinski CA. Lead- and drug-like compounds: the rule-of-five revolution. Drug Discov. Today Technol 2004 Dec; 1 (4):337–341. https://doi.org/10.1016/j.ddtec.2004.11.007
[26] Srimai V, Ramesh M, Parameshwar KS, Parthasarathy T. Computer-aided design of selective Cytochrome P450 inhibitors and docking studies of alkyl resorcinol derivatives. Med Chem Res 2013 Feb; 22: 5314–5323. https://doi.org/10.1007/s00044-013-0532-5
[27] Zhao YH, Abraham MH, Le J, Hersey A, Luscombe CN, Beck G, Sherborn B, Cooper I. Rate-limited steps of human oral absorption and QSAR studies. Pharm Res 2002 Oct; 19: 1446–1457. https://doi.org/10.1023/A:1020444330011
[28] Hebert MF (2013) Impact of pregnancy on maternal pharmacokinetics of medications. Clinical Pharmacology during Pregnancy, Amsterdam, Boston: Academic Press, pp.17–39.
[29] Husain A, Ahmad A, Khan SA, Asif M, Bhutani R, Al-Abbasi FA. Synthesis, molecular properties, toxicity and biological evaluation of some new substituted imidazolidine derivatives in search of potent anti-inflammatory agents. Saudi Pharm. J. 2016 Jan; 24 (1):104–114. https://doi.org/10.1016/j.jsps.2015.02.008